MICROSTRUCTURE EVOLUTION OF 20CR STEEL SPIDER DURING COLD FORGING USING CELLULAR AUTOMATON METHOD

Kun Xia Wei[1,2,4,5], Ling Niu[1,2,4], Wei Wei[1,2,4,5]*, Qing Bo Du[1,2,4,5], Igor V. Alexandrov[3,4], Jing Hu[1,2,4,5]

[1] School of Materials Science and Engineering, Changzhou University, Changzhou 213164, P. R. China
[2] Jiangsu Key Laboratory of Materials Surface Science and Technology, Changzhou University, Changzhou 213164, P.R. China
[3] Department of Physics, Ufa State Aviation Technical University, 12 K. Marx St., 450008 Ufa, Russia
[4] Sino-Russia Joint Laboratory of Functional Nanostructured Materials, Changzhou University, Changzhou 213164, P. R. China
[5] National Experimental Demonstration Center for Materials Science and Engineering (Changzhou University) Changzhou, 213164, P.R. China

*Corresponding author: e-mail:benjamin.wwei@163.com (W. Wei), Tel.:+86 519 8633 0095, School of Materials Science and Engineering, Changzhou University, Changzhou 213164, P. R. China

Abstract

The microstructure evolution of 20Cr steel spider in the cold forging process was simulated and analyzed by the CA method, and verified by the experimental results. The CA simulation results show that the grain size becomes smaller with an increase of forging reduction. When the forging reduction is 60%, the grain size is the smallest. After that, the microstructure is inhomogeneous. At the same forging reduction, the microhardness at the root of the pin is higher than that at the head of the pin. It is well agreed with the distribution of the effective strain. The CA results agree well with the experimental data in terms of microstructure evolution and microhardness distribution, suggesting that the CA model is a reliable numerical approach for predicting microstructure evolution during cold forging for 20Cr steel spider.

Keywords: spider; cellular automaton (CA) method; microstructure evolution; microhardness

1   Introduction

Spider is one of important safety parts of tripod constant velocity (TCV) universal joint, which provides lower plunging resistance in comparison to ball-type joint [1]. Cold precision forging as the main near-net-shape technique is the most popular technology for producing the complex parts, such as worm gear, spider, shaft, turbine, inner and outer race *etc*. due to the lack of flash, the minimum machining allowances and the good service properties [2-4]. The influence of the material ductility and the friction, the punch taper angle on spider cold forging was carried out by 3D finite element methodology [5-7]. In the cold forging process of spider, the grains flow along the different slip direction and slip system. The resistance to the motion of grains is not identical, leading to inhomogeneous deformation microstructure.

As an algorithm describing the discrete spatial and/or temporal microstructure evolution by applying local or global deterministic or probabilistic transformation rules, the cellular automaton (CA) method has been successfully applied to simulate the static recrystallization (SRX), dynamic recrystallization (DRX) and metaynamic recrystallization (MDRX) [8-10]. Coupled with finite element model or macroscopic hot working parameters, the CA is capable of simulating the microstructure evolution at multi-scale [10-13]. However, there is less information available on the microstructure evolution of 20Cr steel during cold forging.

Thus the present work is to investigate the microstructure evolution of 20Cr steel spider in cold forging process based on a CA approach and the actual experiments. The CA simulation results were validated by the metallographic microstructure and the microhardness tests.

2   Model building and simulation control
2.1 Materials model
The spider billet is 20Cr steel with the diameter of 32 mm, the length of 56 mm. The forging die is Cr12MoV steel. The 20Cr steel chemical composition (mass fraction, %) is shown in **Table 1**. The flow stress of the billet follows the equation:

$$\bar{\sigma} = (688 + 92\bar{\varepsilon}^{0.7}) * (1 + 0.0004\ln\dot{\bar{\varepsilon}}) * \left[1 - \left(\frac{T-20}{1300}\right)^{1.1}\right] \tag{1.}$$

Fig. 1 shows the spider part drawing. The small chamfer, rounded corner may be neglected without loss of calculation accuracy. The billet assumed as the elastic-plastic model is defined as the deformation body, and the die is defined as the rigid body.

Table 1 Chemical composition of 20Cr steel

chemical composition (wt.%）							
C	Si	Mn	P	S	Cr	Ni	Cu
0.20	0.23	0.68	0.19	0.03	0.79	0.02	0.02
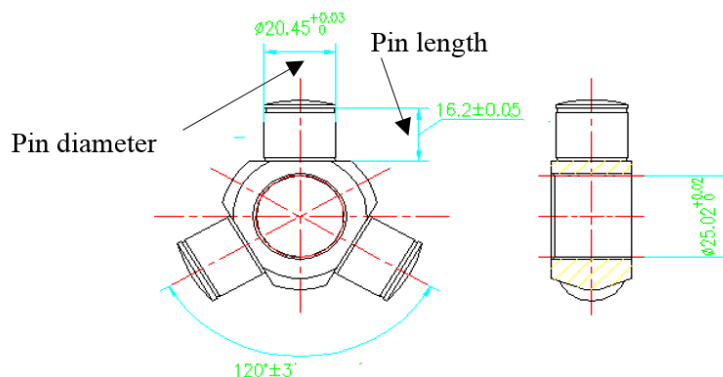
Fig. 1   A drawing of spider part

2.2 Mathematical model of CA method
(1) Dislocation density model

The dislocation density is expressed by an incremental form in DEFORM 3D software.

$$d\rho = (h - r\rho_i)d\varepsilon \qquad (2.)$$

$$h = h_0 \left(\frac{\dot{\varepsilon}}{\dot{\varepsilon}_0}\right)^m exp\left(\frac{mQ}{RT}\right) \qquad (3.)$$

$$r = r_0 \left(\frac{\dot{\varepsilon}}{\dot{\varepsilon}_0}\right)^{-m} exp\left(\frac{-mQ}{RT}\right) \qquad (4.)$$

ρ_i is dislocation density, ε is the strain, h is the range height of dislocation stress field, r is the range radius of stress field, m is the strain rate sensitivity, $\varepsilon^{\cdot}$ is the strain rate, $\dot{\varepsilon}_0$ is the initial dynamic strain rate.

(2) Recovery model

Dynamic recovery is a softening effect due to dynamic annihilation of dislocations in the plastic deformation process. A recovery model proposed by Goetz and Seetharaman is applied in the DEFORM 3D software [14, 15]. Dynamic recovery is modeled by randomly choosing a certain cellular number, *N*, of cells at each step and makes the dislocation density in these cells reduced by one half.

$$\rho_{i,j} = \rho_{i,j}^{t-1}/2 \qquad (5.)$$

Which will make the distribution of dislocations inhomogeneous. The *N* value is determined by the formula:

$$N = \left(\frac{\sqrt{2}m}{K}\right)^2 * \dot{\rho}^2 \qquad (6.)$$

M is the total cell number, K is a constant, $\dot{\rho}$ is the growth rate of dislocation density.

(3)Recrystallization model

It is generally accepted that DRX occurs only when dislocation density or strain reaches a critical value. Nucleation and grain growth during DRX are closely related to the dislocation density, i.e., the variation of stored strain energy in deformed grains and in newly formed grains. Three assumptions are accepted in the present study [16, 17]. (i) Dislocation density is uniform and identical for all the primary grains. The dislocation density evolves from zero to a saturated value in the dynamic recrystallized grains with continued deformation. (ii) Nucleation of DRX takes place only on grain boundaries (including the primary grain boundaries and dynamic recrystallized gain boundaries). (iii) There is no dislocation gradient from the center to the borders of each grain. A series of empirical equations proposed by Kopp were adopted in CA simulation [18].

2.3 Simulation control of spider forging process

CA model is a time and space discretization algorithm, which is necessary to discretely deal with the dislocation density and grain orientation in the simulation process. The simulation lattice was 1000×1000, and the periodic boundary conditions were used. The size of one lattice represents 1

µm of the real dimension of the material, and hence the simulation area corresponds to 1×1 mm^2 in a real sample. The dislocation density parameters are shown in **Table 2**.

Table 2 Dislocation density parameters

parameter	value
initial dynamic strain rate $\dot{\varepsilon}_0$ (s^{-1})	1
Q (J·mol^{-1})	260000
h_0 (mm)	0.00075
r_0 (mm)	2000
K	6030
m_0 (s^{-1})	0.2

3   Results and discussion

Fig. 2 is the simulated microstructure of 20Cr steel in cold forging with different forging reduction of 0%, 25%, 50%, 60%, 75% and 100%. Different colors represent different grains, and the larger the color contrast means that the difference of orientations is larger. It can be seen that the intersection of the grain boundaries is in the triangular shape. In the initial deformation, the grain size is coarse. With an increase of forging reduction, the grain size becomes smaller.
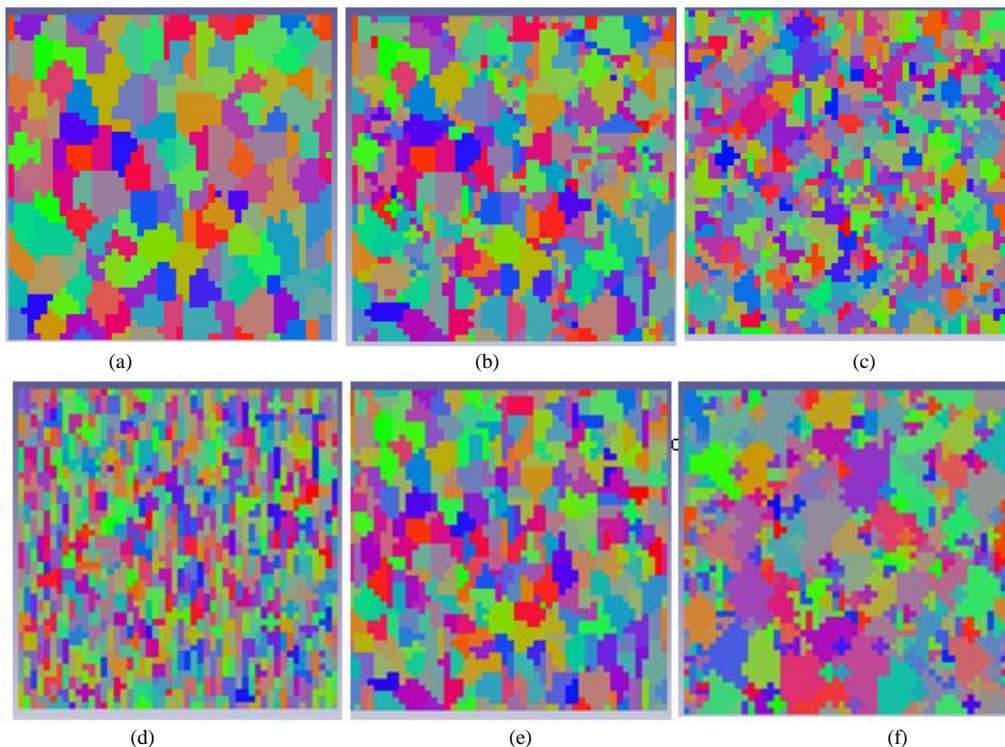
Fig. 2   Simulated microstructure of 20Cr steel in cold forging with different forging reduction: (a) 0%, (b) 25%, (c) 50%, (d) 60%, (e) 75% and (f) 100%

When the reduction is 60%, the grain size is the smallest. After that, the inhomogeneous microstructure is observable, leading to an increase in the average grain size. The average grain size in different deformation stages is listed in **Table 3**. The measured deformation temperature is about 400 ℃ in the cold forging of 20Cr steel spider [19]. In the local part of spider, the deformation temperature may be much higher, some recrystallization occurs. Therefore some coarse grains may be attributed to partial recrystallization after forging reduction of 60%.

Table 3 Average grain size of 20Cr steel spider in different forging reduction using CA method

Forging reduction （％）	Average grain size （μm）
0%	4.01
25%	2.65
50%	2.39
60%	1.90
75%	2.29
100%	3.21

4　Validation of the model
4.1　Optical microstructure

20Cr steel billet was annealed at 780 °C for 5h, then cooled to 500 °C in furnace, finally cooled in air. **Fig. 3** shows the positions of optical observations and microhardness test in the same cross section of spider.
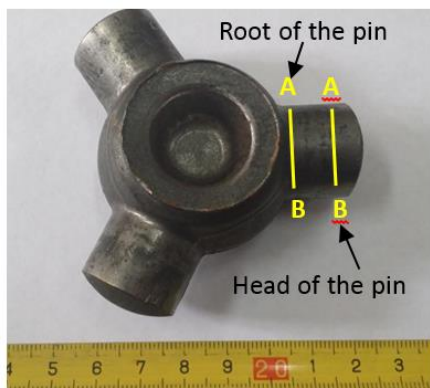
Fig. 3　The positions of optical observation and microhardness tests
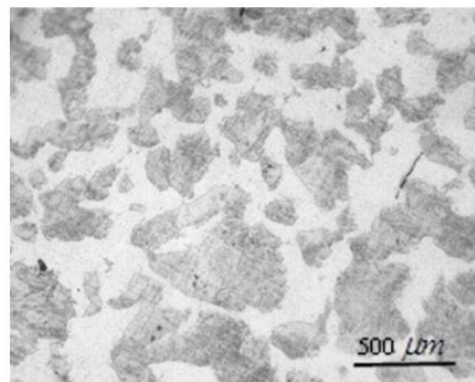
Fig. 4　Optical micrograph of 20Cr steel in the initial state

The actual optical micrographs are shown in Figs. 4-6. The coarse grains in the initial state were gradually refined. The microstructure is small and uniform. When the forging reduction increases to a certain extent, some grains become coarse; others are small, which leads to the microstructure inhomogeneous. This result is consistent with the simulation results in Fig. 2 and Table 3. Due to the lower deformation degree at the head of the pin than that at the root, the corresponding grain size at the head of the pin is lightly bigger than that at the root of the pin.
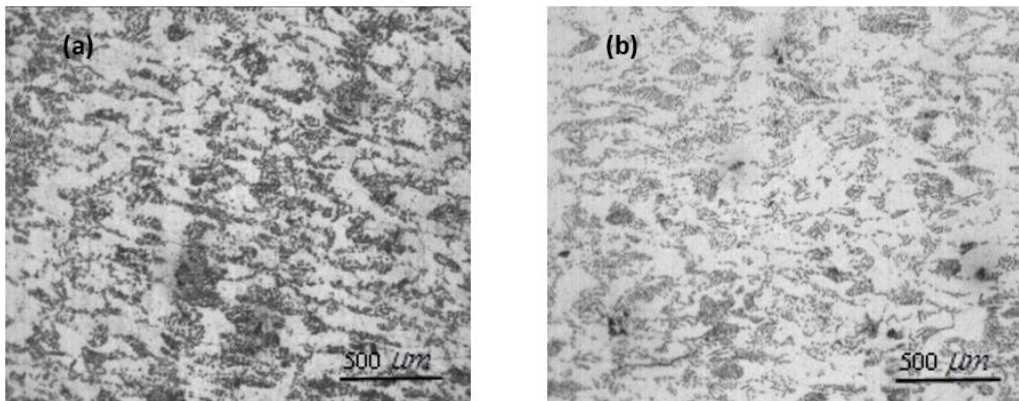
Fig. 5   Optical micrographs of 20Cr steel spider in the forging reduction 50%: (a) the root of the pin, (b) the head of the pin.
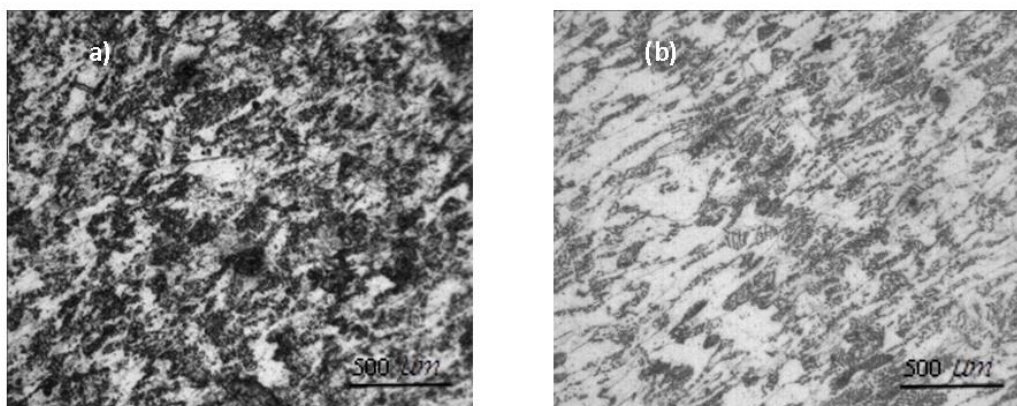
Fig. 6   Optical micrographs of 20Cr steel spider in the forging reduction 100%: (a) the root of the pin, (b) the head of the pin.

4.2 Microhardness

In the cold forging process, microhardness will be increased with the plastic strains. Inhomogeneous plastic deformation will result in the non-uniform distribution of hardness. It is easy to crack for the local part with a higher hardness. Microhardnes was measured by using HVS-5Z with a load of 300 g for 15 sec along the pin diameter direction.

The microhardness of 20Cr steel spider at the root and head of the pin with different forging reduction are shown in **Fig. 7**. It is seen that the microhardness of the pin after the forging reduction of 100% is bigger than that after the forging reduction of 50%. At the same forging reduction, the microhardness at the root of the pin is higher than that at the head of the pin. The variation of microhardness at the root of the pin is not more fluctuated. On the contrary, the microhardness at the head of the pin increases with the distances form the point A to B.

The microhardness will increase with a decrease of the grain size. **Fig. 8** shows that the effective strain at the root of the pin is higher than that at the head of the pin. The higher the forging reduction, the smaller the grain size and the higher dislocation density. This results in a higher microhardness.
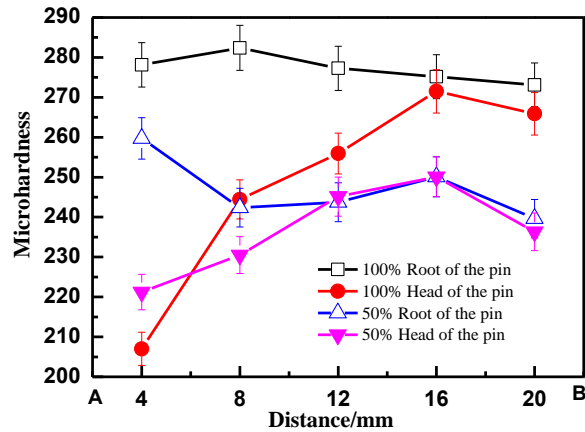
Fig. 7   Microhardness of 20Cr steel spider pin with different forging reduction
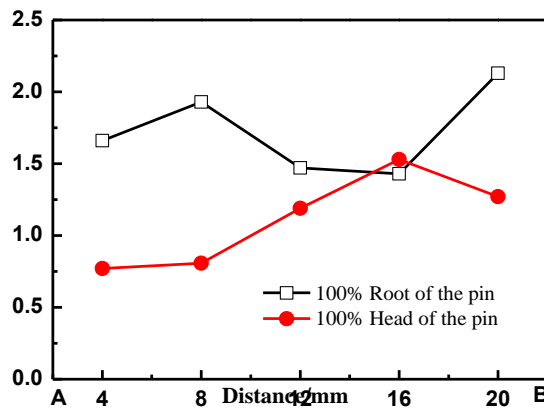
Fig. 8   Effective strain of 20Cr steel spider at the root and head of pin with the forging reduction of 100%
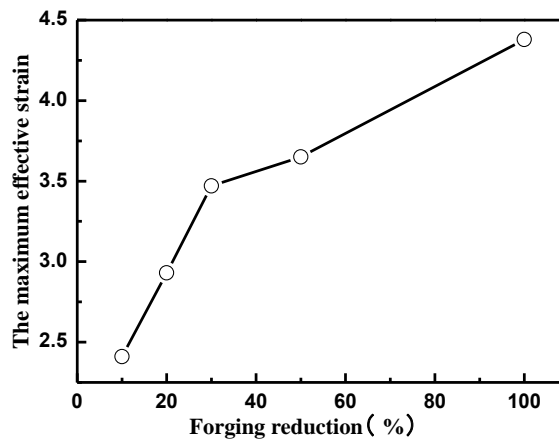
Fig. 9   The relationship of the maximum effective strain and the forging reduction

Fig. 9 shows that with an increase of forging reduction, the maximum effective strain is gradually increasing. The grain size becomes smaller, which can be seen from the CA simulations in **Fig. 2** and the experimental results in **Figs. 4-6**. Therefore, the microhardness of the pin after the forging reduction of 100% is generally larger than that after the forging reduction of 50% in **Fig. 7**.

5   Conclusions

1. Microstructure evolution of 20Cr steel spider was successfully conducted by the CA approach.
2. The CA simulation results show that the grain size becomes smaller with an increase of forging reduction. When the reduction is 60%, the grain size is the smallest. After that, the microstructure is inhomogeneous.
3. The microhardness of the pin after the forging reduction of 100% is bigger than that after the forging reduction of 50%. At the same forging reduction, the microhardness at the root of the pin is higher than that at the head of the pin. It is well agreed with the distribution of the effective strain.

References

[1] F. Schmelz, CH-C Seherr-Thoss, E. Aucktor: Universal joints and driveshafts: analysis, design, applications (translated by SJ Hill and JA Tipper), New York, Springer, 1992

[2] K. Lange: Journal of Materials Processing Technology, Vol. 35, 1992, No. 3-4, p. 245-257, DOI: 10.1016/0924-0136(92)90321-I

[3] S. Onodera, K. Sawai: Journal of Materials Processing Technology, Vol. 35, 1992, No. 3-4, p. 385-396, DOI: 10.1016/0924-0136(92)90329-Q

[4] Z. Gronostajski, M. Hawryluk: Archives of Civil and Mechanical Engineering, Vol. 8, 2008, No. 2, p. 39-55, DOI: 10.1016/S1644-9665(12)60192-7

[5] A. Cherouat, K. Saanouni, Y. Hammi: Journal of Materials Processing Technology, 2003, Vol. 142, No. 2, p. 307-317, DOI: 10.1016/S0924-0136(03)00580-6

[6] J.M. Yan, C.Y. Wang, W. Li, Z.C. Tian, H.E. Zhang: Forging & Stamping Technology, Vol. 38, 2013, No. 2, p. 81-84, DOI: 10.3969/j.issn.1000-3940.2013.02.021

[7] A. Fedorikova, T. Kvackaj, R. Kocisko, R. Bidulsky, P. Petrousek, J. Bidulska, L. Domovcova: Acta Metallurgica Slovaca, Vol. 22, 2016, No. 2, p. 102-110, DOI: 10.12776/ams.v22i2.616

[8] D. Raabe: Annual Review of Materials Research, Vol. 32, 2002, p. 53-76, DOI: 10.1146/annurev.matsci.32.090601.152855

[9] Namin Xiao, Chengwu Zheng, Dianzhong Li , Yiyi Li: Computational Materials Science, Vol. 41, 2008, No.3, p. 366-374, DOI: 10.1016/j.commatsci.2007.04.021

[10] J. Majta, L. Madej, D.S. Svyetlichnyy, K. Perzynski, M. Kwiecien, K.Muszka: Materials Science & Engineering A, Vol. 671, 2016, p. 204-213, DOI: 10.1016/j.msea.2016.06.052

[11] L. Madej, M. Sitko, K. Radwanski, R. Kuziak: Materials Chemistry and Physics, Vol. 179, 2016, p. 282-294, DOI: 10.1016/j.matchemphys.2016.05.040

[12] E. Popova, Y. Staraselski, A. Brahme, R.K. Mishra, K. Inal: International Journal of Plasticity, Vol. 66, 2015,p. 85-102, DOI: 10.1016/j.ijplas.2014.04.008

[13] P. Petrousek, R. Kocisko, T. Kvackaj, R. Bidulsky, J. Bidulska, A. Fedorikova, P. Sabol: Acta Physica Polonica A, Vol. 131, 2017, No. 5, p. 1344-1346, DOI: 10.12693/APhysPolA.131.1344

[14] R.L. Goetz, V. Seetharaman: Scripta Materialia, Vol. 38, 1998, No. 3, p. 405-413, DOI: 10.1016/S1359-6462 (97) 00500-9

[15] R.L. Goetz, V. Seetharaman: Metallurgical and Materials Transactions A, Vol. 29, 1998, No. 9, p. 2307-2321, DOI: org/10.1007/s11661-998-0108-z

[16] R. Ding, Z.X. Guo: Computational Materials Science, Vol. 23, 2002, No. 1-4, p. 209-218, DOI: 10.1016/S0927-0256 (01)00211-7

[17] F. Chen, K. Qi, Z.S. Cui, X.M. Lai: Computational Materials Science, Vol. 83, 2014, p. 331-340, DOI: 10.1016/j.commatsci.2013.11.029

[18] R. Kopp, K. Karhausen: Steel Research, Vol. 63, 1992, No. 6, p. 247-266, DOI: 10.1002/srin.199200509

[19] L. Niu, W. Wei, K.X. Wei, I.V. Alexandrov, J. Hu: Journal of Materials Engineering and Performance, Vol. 25, 2016, No. 6, p. 2536-2541, DOI: 10.1007/s11665-016-2108-2